applied optics

Grating design for interlayer optical interconnection of in-plane waveguides

CONGSHAN WAN, THOMAS K. GAYLORD, AND MUHANNAD S. BAKIR*

School of Electrical and Computer Engineering, Georgia Institute of Technology, Atlanta, Georgia 30332, USA
**Corresponding author: muhannad.bakir@mirc.gatech.edu*

Received 8 January 2016; revised 23 February 2016; accepted 24 February 2016; posted 24 February 2016 (Doc. ID 257020); published 25 March 2016

Interlayer grating-to-grating optical interconnect coupling efficiency is simulated and optimized using rigorous coupled-wave analysis (RCWA) for the case of binary rectangular-groove gratings. The "equivalent index slab (EIS)" concept is proposed to alleviate the numerical sensitivity problem inherent in the RCWA-leaky-wave approach, making the method applicable to any multilayer structure that has an arbitrary grating profile, large refractive-index differences, and a limited grating length. The method is easy to implement and computationally efficient and can provide optimal designs based on the system designer's need. To determine the viability of the RCWA-EIS approach, results are compared to those obtained using the finite-difference time-domain method, and an excellent agreement is found.

OCIS codes: (050.1950) Diffraction gratings; (050.1960) Diffraction theory; (060.1810) Buffers, couplers, routers, switches, and multiplexers; (130.0130) Integrated optics; (250.5300) Photonic integrated circuits.

http://dx.doi.org/10.1364/AO.55.002601

1. INTRODUCTION

Optical interconnects have demonstrated their indispensable role in monolithic integration with electrical interconnects to meet the ever growing needs of terabit per second data rates driven by modern computing systems. Compared to electrical links, optical interconnects, which have many practical benefits such as high bandwidth density, low energy dissipation, and low communication latency, offer a promising solution for large-scale integration. As more optical components are integrated, single-layer structures with an increasing number of waveguides would eventually suffer from unacceptable cross talk and loss. The development of multilayer platforms with out-of-plane interlayer optical connectors appears to be inevitable, as they provide rerouting capability to avoid high waveguide densities and waveguide crossings. Diffraction gratings, as compact optical connectors, play vital roles in determining the optical link scale. Designing high-efficiency grating-to-grating couplers and consequently extending the interconnect scale have become important research topics in the fields of interconnects and packaging.

A number of approaches are available to analyze the grating diffraction phenomenon, such as coupled-wave approaches [1,2], modal approaches [3], perturbation methods [4,5], integral methods [6], differential methods [7], transmission line equivalent network approaches [5,8], amplitude transmittance approaches [9–11], coupled-mode approaches [12,13], and rigorous coupled-wave analysis (RCWA) methods [14,15]. Among all of these methods, RCWA is accurate and computationally efficient. Previous work with RCWA has primarily focused on the diffraction analysis of grating structures with little emphasis on in-coupling into guided waves. The RCWA-leaky-wave (RCWA-LW) approach [16–18] was proposed to analyze the out-diffraction of a guided wave via a grating, but its application is limited to grating structures with small refractive-index differences. Existing optimization efforts have mostly focused on fiber-to-grating coupling using advanced search algorithms [19,20]. Only a limited number of papers have discussed grating-to-grating coupling. The first preferential-order optical couplers on different substrates were demonstrated in [21], but this work utilized volume gratings, and no optimization process was provided. Compared with volume gratings, surface-relief gratings have reduced the thickness and improved process integration, thus becoming a popular solution in compact interconnect technology. Recent optimization work on interlayer surface-relief grating coupling used the finite-difference time-domain (FDTD) [22,23], COMSOL multiphysics [24], or CAMFR simulation package [25] as the starting point to design the gratings, which can be a very time-consuming process. There are several papers using a grating design for a specific structure [26,27], but which do not include any optimization analysis or trends, providing little information on designing a distinctly different structure with differing materials. Sodagar *et al.* [28] used a MATLAB-implemented genetic algorithm to optimize interlayer gratings. They showed

a fast convergence rate, but the optimization process was not disclosed. Furthermore, this method had limited applicability because it could only optimize two parameters of the rectangular-groove gratings, namely the grating period and fill factor, and the parameters had to be manually changed during optimization based on educated guesses and past experience.

The present work provides a flexible and comprehensive method to optimize the interlayer grating coupling efficiency. The method is easy to use, time efficient, and requires no educated choice of initial parameters. It could optimize a large parameter space given a particular grating profile, which is not limited to a rectangular groove. The interlayer grating coupling problem is schematically depicted in Fig. 1 (a general representation that is not to scale). The guided wave confined in the slab waveguide on the bottom (top) layer is diffracted out via the grating (out-diffraction) and coupled into another slab waveguide on the top (bottom) layer (in-coupling). By the reciprocal theorem [29,30], grating structures with maximized in-coupling efficiency subsequently experience maximum out-diffraction efficiency. Therefore, optimization of a single in-coupling process is sufficient to determine optimal grating designs if the top and bottom gratings are identical. The primary approach in this work is first to use the RCWA approach to represent the field distribution of the waveguide grating structure, then to optimize the input parameter space to get the maximized coupling efficiency, and finally to use FDTD simulation to verify the results. The RCWA approach solves the exact electromagnetic boundary-value problem in a straightforward formulation and gives rapidly converging results. It is assumed that a plane wave is incident from the cover to an infinitely long periodic grating. RCWA can approximate the in-coupling process even though the incident wave, which is the output wave of the out-diffraction process, is exponentially decreasing.

Grating diffraction analysis is a numerically sensitive problem. Previous optimizations of the parameter space were mostly governed by the out-diffraction process modeled by the RCWA-LW approach, which involves an intermediate step to determine a complex propagation constant such that the determinant of the boundary condition matrix is zero [7,16,17]. This intermediate calculation is based on the Muller method, which is very sensitive to initial guesses. Careful choice of the initial guesses is crucial for the Muller method to converge to meaningful results, which is especially difficult to achieve for material systems with large-index differences, thus making this method tedious and less practical. In the present analysis, optimization is done on the in-coupling process, and an "equivalent index slab" method is proposed to determine the radiation factor of the waveguide grating structure under investigation. In this way, solving the determinant of a large-dimension matrix is circumvented, thus extending the applicability of the method to arbitrary material systems.

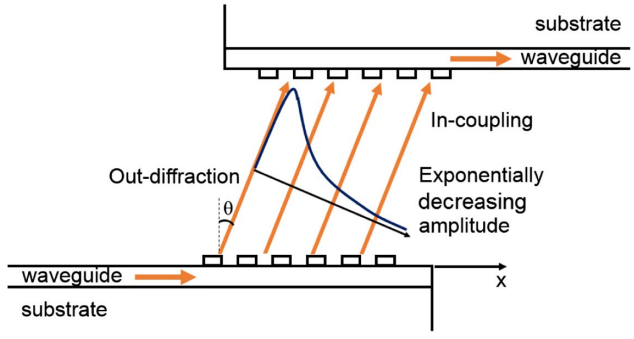

Fig. 1. Schematic representation (not to scale) of a grating-to-grating coupling process. A guided mode confined in the bottom waveguide is incident on the diffraction grating and out-diffracted; the out-diffracted light is incident on the upper grating and coupled into the upper waveguide.

2. GRATING IN-COUPLING MODEL

As shown in Fig. 1, each surface-relief grating consists of a general four-layer structure, namely consisting of the cover, the index modulation layer, the waveguide, and the substrate. In this analysis, a surface-relief grating with a given profile is deposited on a slab dielectric waveguide. This model is also capable of simulating gratings etched into the waveguide. In the following analysis, a TE polarization (y direction) wave propagating in the x direction is considered.

A. Theory and Formulation

The RCWA derivations are based on [14]. As shown in Fig. 2(a), an electromagnetic plane wave with free-space wavelength λ_0 is obliquely incident upon the surface-relief grating at an angle θ. The grating layer is composed of a periodic distribution of grating ridges (with refractive index n_{rd}) and grating grooves (with refractive index n_{gr}), and the fraction of the grating ridge with respect to the whole period Λ is indicated by the fill factor f. For nonbinary grating profiles (arbitrary periodic shapes), the entire grating structure is horizontally sliced into sublayers, which can be approximated as a series of binary gratings with varying fill factors or ridge locations [31,32]. For

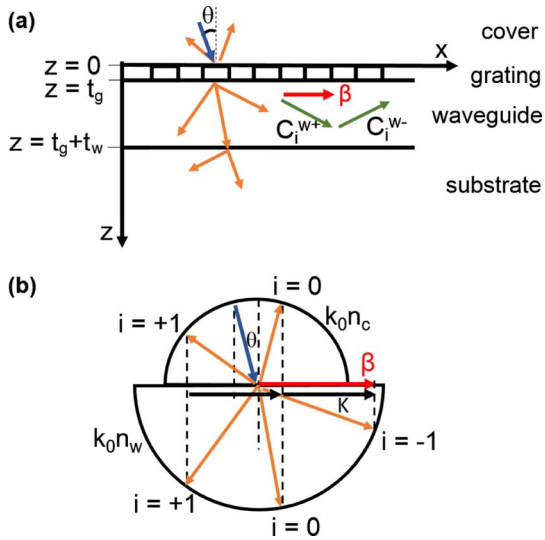

Fig. 2. Schematic representation of (a) the grating in-coupling process and (b) the phase diagram based on the Floquet condition. This example shows multiple diffraction orders in the cover and substrate (not optimized for high efficiency), and the −1 order is a possible guided order whose propagation constant in the x direction is approximately equal to the guided mode propagation constant β in the waveguide.

simplicity, the formulation introduced here will be focused on the binary grating. The relative permittivity of the binary grating can be expanded in a Fourier series along the x direction in the form

$$\epsilon_g(x) = \epsilon_{g0} + (\epsilon_{\mathrm{rd}} - \epsilon_{\mathrm{gr}}) \sum_{\substack{h=-\infty \\ h\neq 0}}^{\infty} \frac{\sin(\pi h f)}{\pi h} \exp(jhKx), \quad (1)$$

where ϵ_{g0} is the average grating permittivity, defined as $\epsilon_{g0} = n_{\mathrm{rd}}^2 f + n_{\mathrm{gr}}^2(1-f)$, and K is the grating vector magnitude ($K = 2\pi/\Lambda$). For the following analysis, $\tilde{\epsilon}_h$ is defined as

$$\tilde{\epsilon}_0 = \epsilon_{g0}, \quad (2)$$

$$\tilde{\epsilon}_h = (\epsilon_{\mathrm{rd}} - \epsilon_{\mathrm{gr}}) \frac{\sin(\pi h f)}{\pi h}. \quad (3)$$

The periodic structure perturbs the incident plane wave into multiple discrete directions indicated by the diffraction orders, and it produces both forward-diffracted waves ($+z$ direction) and backward-diffracted waves ($-z$ direction). Since the incident wave is TE polarized, the electric field has only a y component, while magnetic field has both x and z components. The electric field in the cover is the sum of the incident and backward-diffracted waves. The normalized total electric field in the cover is expressed as

$$E_{cy}(x,z) = \exp[-jk_0 n_c(\sin\theta x + \cos\theta z)] + \sum_i R_i \exp(-jk_{x,i}x + jk_{cz,i}z), \quad (4)$$

and the normalized electric field in the substrate is expressed as

$$E_{sy}(x,z) = \sum_i T_i \exp[-jk_{x,i}x - jk_{sz,i}(z - t_g - t_w)]. \quad (5)$$

The electric field inside the slab waveguide is a superposition of forward-z-propagating waves and backward-z-propagating waves expressed as

$$E_{wy}(x,z) = \sum_i \{C_i^{w+} \exp[-jk_{wz,i}(z - t_g)] + C_i^{w-} \exp[+jk_{wz,i}(z - t_g - t_w)]\} \exp(-jk_{x,i}x), \quad (6)$$

where k_0 is the wavevector magnitude in free space ($k_0 = 2\pi/\lambda_0$); the summation is from $i = -(s-1)/2$ to $(s-1)/2$, where s is the total number of diffraction orders (an odd number for calculation convenience); R_i and T_i are the normalized ith backward-diffracted amplitude (reflected) and forward-diffracted amplitude (transmitted), respectively; t_g and t_w are the grating layer thickness and the waveguide thickness, respectively; $k_{x,i}$ is the ith propagation constant in the x direction, defined by the Floquet condition [Fig. 2(b)]

$$k_{x,i} = k_0 n_c \sin\theta - iK; \quad (7)$$

and $k_{rz,i}$ is the propagation constant in the z direction, defined as

$$k_{rz,i} = \begin{cases} \sqrt{n_r^2 k_0^2 - k_{x,i}^2} & n_r k_0 > |k_{x,i}| \\ -j\sqrt{k_{x,i}^2 - n_r^2 k_0^2} & n_r k_0 < |k_{x,i}|. \end{cases} \qquad r = c, w, s. \quad (8)$$

According to Maxwell's equation $\mathbf{H} = \frac{j}{\omega\mu}\nabla \times \mathbf{E}$, the tangential magnetic fields in the cover, substrate, and waveguide are expressed as

$$H_{cx}(x,z) = \frac{1}{j\omega\mu_0}\left\{-jk_0 n_c \cos\theta \exp[-jk_0 n_c(\sin\theta x + \cos\theta z)] + \sum_i jk_{cz,i}R_i \exp(-jk_{x,i}x + jk_{cz,i}z)\right\}, \quad (9)$$

$$H_{sx}(x,z) = \frac{1}{j\omega\mu_0}\sum_i (-jk_{sz,i}) T_i \exp[-jk_{x,i}x - jk_{sz,i}(z - t_g - t_w)], \quad (10)$$

$$H_{wx}(x,z) = \frac{1}{j\omega\mu_0}\sum_i \{C_i^{w+}(-jk_{wz,i}) \exp[-jk_{wz,i}(z - t_g)] + C_i^{w-}(+jk_{wz,i}) \exp[+jk_{wz,i}(z - t_g - t_w)]\} \times \exp(-jk_{x,i}x). \quad (11)$$

The electric field in the grating region ($0 < z < t_g$) is expressed by a Fourier expansion in spatial harmonics as

$$E_{gy}(x,z) = \sum_i S_{gy,i} \exp(-jk_{x,i}x), \quad (12)$$

and the tangential magnetic field in the grating region is derived from Maxwell's equation as

$$H_{gx}(x,z) = -j\sqrt{\frac{\epsilon_0}{\mu_0}}\sum_i U_{gx,i} \exp(-jk_{x,i}x), \quad (13)$$

where $U_{gx,i} = \frac{1}{k_0}\frac{\partial S_{gy,i}}{\partial z}$. Equation (12) satisfies the wave equation for TE polarization in the grating region,

$$\nabla^2 E_{gy} + k_0^2 \epsilon_g(x) E_{gy} = 0. \quad (14)$$

Equation (12) is substituted into Eq. (14), and the following equation can be derived:

$$\frac{\partial^2 S_{gy,i}}{\partial z^2} + (k_0^2 \epsilon_g - k_{x,i}^2) S_{gy,i} = 0, \quad (15)$$

which can be written in a matrix

$$\left[\frac{\partial^2 \mathbf{S}_{gy}}{\partial (z')^2}\right] = [\mathbf{A}_g][\mathbf{S}_{gy}], \quad (16)$$

where $z' = k_0 z$ and $\mathbf{A}_g = \mathbf{K}_x^2 - \mathbf{E}_g$; $\mathbf{K}_x$ is a diagonal matrix with the (i,i) element being k_{xi}/k_0, and $\mathbf{E}_g$ is the matrix of the permittivity coefficient $\tilde{\epsilon}_h$ [Eqs. (2) and (3)], defined as

$$\mathbf{E}_g = \begin{bmatrix} \ddots & \vdots & \vdots & \vdots & \iddots \\ \cdots & \tilde{\epsilon}_0 & \tilde{\epsilon}_{-1} & \tilde{\epsilon}_{-2} & \cdots \\ \cdots & \tilde{\epsilon}_1 & \tilde{\epsilon}_0 & \tilde{\epsilon}_{-1} & \cdots \\ \cdots & \tilde{\epsilon}_2 & \tilde{\epsilon}_1 & \tilde{\epsilon}_0 & \cdots \\ \iddots & \vdots & \vdots & \vdots & \ddots \end{bmatrix}. \quad (17)$$

For a binary grating whose grating profile is symmetric, $\mathbf{E}_g$ is a symmetric matrix ($\tilde{\epsilon}_{-h} = \tilde{\epsilon}_h$).

Equation (16) is a typical second-order homogeneous system of differential equations, and its solution can be expressed by the eigenvalues and eigenvectors of matrix $\mathbf{A}_g$. As a result, the space harmonic expansions of the tangential electric and magnetic fields in the grating are expressed as

$$S_{gy,i}(z) = \sum_{p=1}^{s} w_{i,p}^{g}\{C_p^{g+}\exp(-k_0 q_p^g z) + C_p^{g-}\exp[k_0 q_p^g (z - t_g)]\}, \tag{18}$$

$$U_{gx,i}(z) = \sum_{p=1}^{s} v_{i,p}^{g}\{-C_p^{g+}\exp(-k_0 q_p^g z) + C_p^{g-}\exp[k_0 q_p^g (z - t_g)]\}, \tag{19}$$

where $w_{i,p}^g$ is the (i, p) element of the eigenvector matrix $\mathbf{W}_g$, and q_p^g is the positive square root of the (p, p)th element of the eigenvalue matrix $\mathbf{Q}_g$. According to Eq. (13), it can be found that $v_{i,p}^g = w_{i,p}^g q_p^g$, and, therefore, $\mathbf{V}_g = \mathbf{W}_g\mathbf{Q}_g$. C_p^{g+} and C_p^{g-} are unknown coefficients, which will be determined from the boundary conditions. The $\exp(-k_0 q_p^g z)$ term represents forward-propagating $(+z)$ waves, and the $\exp[k_0 q_p^g (z - t_g)]$ term represents backward-propagating $(-z)$ waves in the grating region.

The coefficients R_i, C_p^{g+}, C_p^{g-}, C_i^{w+}, C_i^{w-}, and T_i for the cover, grating, waveguide, and substrate can be determined by matching the tangential electric field E_y [Eqs. (4), (12), (6), and (5)] and the tangential magnetic field H_x [Eqs. (9), (13), (11), and (10)] at all boundaries. At $z = 0$ (the boundary between the cover and the grating),

$$\begin{bmatrix} \delta_{i0} \\ jn_c\cos\theta\delta_{i0} \end{bmatrix} + \begin{bmatrix} \mathbf{I} \\ -j\mathbf{Y}_c \end{bmatrix}\begin{bmatrix} \mathbf{R} \end{bmatrix} = \begin{bmatrix} \mathbf{W}_g & \mathbf{W}_g\mathbf{X}_g \\ \mathbf{V}_g & -\mathbf{V}_g\mathbf{X}_g \end{bmatrix}\begin{bmatrix} \mathbf{C}_g^+ \\ \mathbf{C}_g^- \end{bmatrix}; \tag{20}$$

at $z = t_g$ (the boundary between the grating and waveguide),

$$\begin{bmatrix} \mathbf{W}_g\mathbf{X}_g & \mathbf{W}_g \\ \mathbf{V}_g\mathbf{X}_g & -\mathbf{V}_g \end{bmatrix}\begin{bmatrix} \mathbf{C}_g^+ \\ \mathbf{C}_g^- \end{bmatrix} = \begin{bmatrix} \mathbf{I} & \mathbf{X}_w \\ j\mathbf{Y}_w & -j\mathbf{Y}_w\mathbf{X}_w \end{bmatrix}\begin{bmatrix} \mathbf{C}_w^+ \\ \mathbf{C}_w^- \end{bmatrix}; \tag{21}$$

and at $z = t_g + t_w$ (the boundary between the waveguide and the substrate),

$$\begin{bmatrix} \mathbf{X}_w & \mathbf{I} \\ \mathbf{X}_w & -\mathbf{I} \end{bmatrix}\begin{bmatrix} \mathbf{C}_w^+ \\ \mathbf{C}_w^- \end{bmatrix} = \begin{bmatrix} \mathbf{I} \\ \mathbf{Y}_{s/w} \end{bmatrix}\begin{bmatrix} \mathbf{T} \end{bmatrix}, \tag{22}$$

where $\mathbf{X}_g$, $\mathbf{X}_w$, $\mathbf{Y}_c$, $\mathbf{Y}_w$, and $\mathbf{Y}_{s/w}$ are diagonal matrices with diagonal elements $\exp(-k_0 q_p^g t_g)$, $\exp(-jk_{wz,i}t_w)$, $k_{cz,i}/k_0$, $k_{wz,i}/k_0$, and $k_{sz,i}/k_{wz,i}$, respectively.

The matrix equations can be merged into a nonhomogeneous system of equations represented by $\mathbf{Mx} = \mathbf{b}$, and the field amplitudes $\mathbf{x}$ can be calculated by $\mathbf{x} = \text{inv}(\mathbf{M})\mathbf{b}$. The matrix inversion can be calculated by $\text{inv}(\mathbf{M}) = \mathbf{V}(1/\mathbf{S})\mathbf{U}'$, where $\mathbf{U}$, $\mathbf{S}$, and $\mathbf{V}$ are obtained from the singular value decomposition $\mathbf{M} = \mathbf{USV}'$. The amplitudes can also be determined by a transfer matrix approach introduced in [31].

B. "Equivalent Index Slab (EIS)" Approximation for Diffraction Efficiency Calculation

Since RCWA describes the response due to a plane wave incident upon a multilayer structure with infinite boundaries along the x direction, power conservation is only fulfilled in the z direction, which is perpendicular to the infinite boundaries, while power flow in the x direction is not involved in the power conservation. This poses a difficulty when determining the amount of power coupled into the guided mode in the x direction. As a result, we need to take advantage of the light reciprocity and use the out-diffraction process to calculate indirectly the in-coupling diffraction efficiency. As illustrated in Fig. 3(a), the in-coupling efficiency to the +1 order in Fig. 3(a) is the same as the out-diffraction efficiency to +1 order in Fig. 3(b).

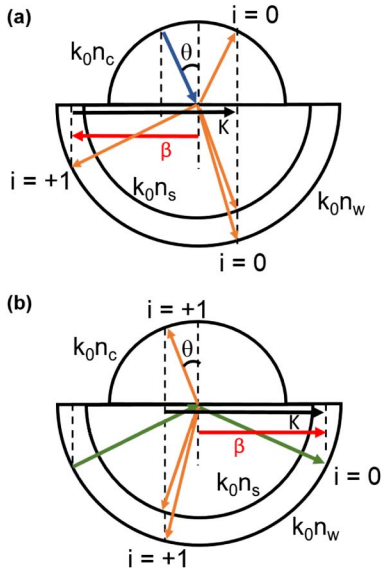

Fig. 3. Phase diagram of (a) the grating in-coupling and (b) the out-diffraction process with only the 0 and +1 orders. The light in-coupling into the +1 order in (a) is the reciprocal process of the guided wave out-diffraction into the +1 order in (b).

Previous work [16–18] attempted to solve the out-diffraction efficiency by removing the incident light contribution [δ_{i0} in Eq. (20)] and casting the problem into a homogeneous system of equations in the form of

$$\begin{bmatrix} -\mathbf{I} & \mathbf{0} & \mathbf{W}_g & \mathbf{W}_g\mathbf{X}_g & \mathbf{0} & \mathbf{0} \\ j\tilde{\mathbf{Y}}_c & \mathbf{0} & \mathbf{V}_g & -\mathbf{V}_g\mathbf{X}_g & \mathbf{0} & \mathbf{0} \\ \mathbf{0} & \mathbf{0} & \mathbf{W}_g\mathbf{X}_g & \mathbf{W}_g & -\mathbf{I} & -\mathbf{X}_w \\ \mathbf{0} & \mathbf{0} & \mathbf{V}_g\mathbf{X}_g & -\mathbf{V}_g & -j\tilde{\mathbf{Y}}_w & j\tilde{\mathbf{Y}}_w\mathbf{X}_w \\ \mathbf{0} & -\mathbf{I} & \mathbf{0} & \mathbf{0} & \mathbf{X}_w & \mathbf{I} \\ \mathbf{0} & -\tilde{\mathbf{Y}}_{s/w} & \mathbf{0} & \mathbf{0} & \mathbf{X}_w & -\mathbf{I} \end{bmatrix}\begin{bmatrix} \mathbf{R} \\ \mathbf{T} \\ \mathbf{C}_g^+ \\ \mathbf{C}_g^- \\ \mathbf{C}_w^+ \\ \mathbf{C}_w^- \end{bmatrix} = \begin{bmatrix} \mathbf{0} \\ \mathbf{0} \\ \mathbf{0} \\ \mathbf{0} \\ \mathbf{0} \\ \mathbf{0} \end{bmatrix}, \tag{23}$$

which can be represented by $\mathbf{Mx} = \mathbf{0}$. The problem becomes finding a complex propagation constant $\tilde{\gamma} = \beta - j\alpha$ with an unknown positive real number β and α such that the determinant of the boundary condition matrix $\mathbf{M}$ is minimized (close to zero). As the complex propagation constant is involved in the calculation, Eq. (7) is modified to

$$\tilde{k}_{x,i} = \tilde{\gamma} - iK = (\beta - iK) - j\alpha, \tag{24}$$

and Eq. (8) becomes

$$\tilde{k}_{rz,i} = \begin{cases} \sqrt{n_r^2 k_0^2 - \tilde{k}_{rz,i}^2} & \mathrm{Re}(\tilde{k}_{rz,i}) > \mathrm{Im}(\tilde{k}_{rz,i}) \\ -\sqrt{n_r^2 k_0^2 - \tilde{k}_{rz,i}^2} & \mathrm{Re}(\tilde{k}_{rz,i}) < \mathrm{Im}(\tilde{k}_{rz,i}) \end{cases} \quad r = c, s. \tag{25}$$

Then, $\tilde{\mathbf{Y}}_c$, $\tilde{\mathbf{Y}}_w$, and $\tilde{\mathbf{Y}}_{s/w}$ are defined as $\tilde{k}_{cz,i}/k_0$, $\tilde{k}_{wz,i}/k_0$, and $\tilde{k}_{sz,i}/k_{wz,i}$, respectively. The application of this method is limited to grating structures with small-index modulations (Δn is on the order of 0.01–0.5); however, it is difficult for the algorithm to find a $\tilde{\gamma}$ solution within reasonable boundaries when the index difference is large ($\Delta n > 1$), even though Δn is successively increased from small values to the desired value, and the converged results obtained from the Muller method are used as the initial guesses for the next steps.

Here, we propose the "equivalent index slab (EIS)" method to circumvent the process of minimizing the determinant. In this analysis, the grating is designed to couple the $i = +1$ order diffracted wave into the waveguide, which ensures the minimum number of propagating orders in the cover and the substrate and thus maximizes diffraction efficiencies, as shown in Fig. 3. All fields in the structure, as well as the propagation constants, can be determined from the in-coupling process. By reciprocity, in-coupled light and out-diffracted light should have the same real propagation constant in the x direction, denoted as β. The problem becomes finding the radiation factor α that will be used to calculate the diffraction efficiencies. The grating layer, whose field expansion involves a sum of exponential terms, is replaced by L layers of uniform equivalent slabs with unknown refractive indices, and the electric field expansion in the z direction of the lth slab is

$$E_{ly,i}(z) = C_i^{l+} \exp\{-jk_{lz,i}[z - (l-1)t_l]\} + C_i^{l-} \exp[+jk_{lz,i}(z - lt_l)], \tag{26}$$

where $t_l = t_g/L$, and L is an arbitrary positive integer ($L \geq 4$). With only two diffraction orders (0 and +1) involved, the only requirement for definition of the equivalent slabs is matching the field amplitudes R_0 and R_1 at the cover-grating interface and C_0^{w+}, C_0^{w-}, C_1^{w+}, and C_1^{w-} at the grating-waveguide interface. As shown in Fig. 4, the equivalent slabs generate the same fields outside grating region, even though the field distributions inside the grating region may vary. Retaining the field profiles in the cover and the waveguide is important because the radiation losses are mainly due to the radiation in the cover and the substrate. Similar to a "black box," the complicated field expansion inside of the "box" is replaced by simple expressions, while the outside fields remain unchanged. The EIS concept is similar to the method introduced in [33], in which the grating layer is replaced by a homogeneous dielectric slab with a predefined index and then simulated by the transmission line approach. But here, the equivalent slab indices are varied based on the fields outside the gratings.

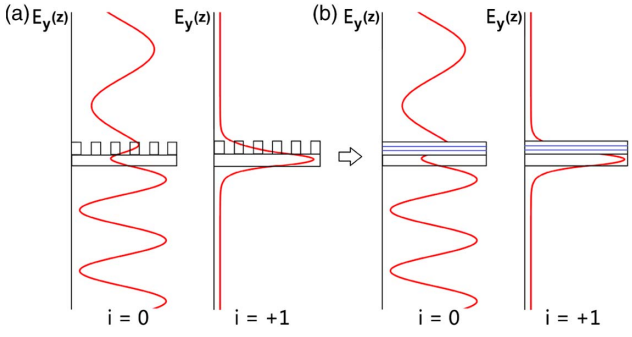

Fig. 4. Schematic representation of field repetition outside of the grating by equivalent index slabs. (a) Electric field amplitude along the z direction of the multilayer grating structure, and (b) equivalent index slabs are used to replace the grating layer. It is not necessary to consider the fields inside the grating region.

The RCWA-EIS approach works well when only two diffraction orders are considered. If more diffraction orders are involved, a larger boundary condition matrix, in the form of Eq. (23), has to be constructed, and the formulation is then no different from the RCWA-LW approach. In that case, there is no point in finding equivalent index slabs to replace the grating. In other words, the RCWA-EIS approach is a simplified version of the RCWA-LW approach relying on multiple equivalent index slabs to represent the grating, and it can only be efficiently used to treat a small number of diffraction orders.

Specifically, by imposing boundary conditions on the electric and magnetic fields, the following transfer matrix formulation can be obtained for the 0th order:

$$\begin{bmatrix} 1 \\ -k_0 n_c \cos(\theta) \end{bmatrix} + \begin{bmatrix} 1 \\ k_{cz,0} \end{bmatrix} R_0 = \prod_{l=1}^{L} \begin{bmatrix} 1 & E_{l,0} \\ -k_{lz,0} & k_{lz,0}E_{l,0} \end{bmatrix} \begin{bmatrix} E_{l,0} & 1 \\ -k_{lz,0}E_{l,0} & k_{lz,0} \end{bmatrix}^{-1} \times \begin{bmatrix} 1 & E_{w,0} \\ -k_{wz,0} & k_{wz,0}E_{w,0} \end{bmatrix} \begin{bmatrix} C_0^{w+} \\ C_0^{w-} \end{bmatrix} = \begin{bmatrix} P_{0,11} & P_{0,12} \\ P_{0,21} & P_{0,22} \end{bmatrix} \begin{bmatrix} C_0^{w+} \\ C_0^{w-} \end{bmatrix}, \tag{27}$$

where $E_{l,0} = \exp(-jk_{lz,0}t_l)$, $E_{w,0} = \exp(-jk_{wz,0}t_l)$, and $k_{lz,0}$ is defined in the same way as in Eq. (8), except for replacing the refractive index with the unknown equivalent slab index n_l. Equation (27) can be transformed into

$$P_{0,11}C_0^{w+} + P_{0,12}C_0^{w-} - 1 - R_0 = 0, \tag{28}$$

$$P_{0,21}C_0^{w+} + P_{0,22}C_0^{w-} - k_{cz,0}R_0 + k_0 n_c \cos(\theta) = 0. \tag{29}$$

The transfer matrix formulation for the +1 order has a similar form as Eq. (27) but excludes the incident light contribution (1 and $k_0 n_c \cos\theta$), and it can be transformed into

$$P_{1,11}C_1^{w+} + P_{1,12}C_1^{w-} - R_1 = 0, \tag{30}$$

$$P_{1,21}C_1^{w+} + P_{1,22}C_1^{w-} - k_{cz,1}R_1 = 0, \tag{31}$$

where $k_{cz,0}$, $k_{wz,0}$, R_0, R_1, C_0^{w+}, C_0^{w-}, C_1^{w+}, and C_1^{w-} are known from the in-coupling calculation.

The problem then becomes finding L equivalent refractive indices such that Eqs. (28)–(31) are satisfied simultaneously. This can be done by using the MATLAB function *fsolve* and restricting function values to be less than 0.01. The algorithm used in *fsolve* is chosen to be the Levenberg–Marquardt method, which is based on the nonlinear least-squares algorithms and can be used if the system may not have a zero. The algorithm still returns a point where the residual is small. Normally, $L = 4$ is enough to achieve the function tolerance.

After the number of equivalent slabs and their corresponding indices are determined, the radiation factor α is determined using a similar process as that discussed in [34]. But here, we will consider two out-diffracted orders with $k_{x,0} = \beta - j\alpha$ and $k_{x,1} = K - \beta - j\alpha$ as propagation constants in the x direction. The sign of the real part of $k_{x,1}$ is not of consequence since $k_{x,1}$ is only used to calculate $k_{cz,1}$, $k_{sz,1}$, and $k_{wz,1}$. The transfer matrix formulations for both orders are in the form of Eq. (27) (without incident light) with the replacement

$$\begin{bmatrix} C_0^{w+} \\ C_0^{w-} \end{bmatrix} = \begin{bmatrix} E_{w,0/1} & 1 \\ -\tilde{k}_{wz,0} E_{w,0/1} & \tilde{k}_{wz,0/1} \end{bmatrix}^{-1} \begin{bmatrix} 1 \\ \tilde{k}_{sz,0/1} \end{bmatrix} T_{0/1} \quad (32)$$

and can be written in a simplified form as

$$\begin{bmatrix} 1 \\ \tilde{k}_{cz,0/1} \end{bmatrix} R_{0/1} = \begin{bmatrix} Q_{0/1,1} \\ Q_{0/1,2} \end{bmatrix} T_{0/1}, \quad (33)$$

which results in $R_{0/1} = Q_{0/1,1} T_{0/1}$, where $0/1$ indicates the 0 or $+1$ order. Therefore, we need to find an α such that $R_0 - Q_0 T_0$ and $R_1 - Q_1 T_1$ are simultaneously close to zero for the existence of an out-diffracted order/in-coupled order. Again, this can be achieved by the MATLAB function *fsolve* with the Levenberg–Marquardt method. Here, the field amplitudes inside the grating are assumed to be the same for the in-coupling and out-diffracted situations, similar to the assumption in the RCWA-LW approach [16–18].

After α is determined, the diffraction efficiency can be calculated by substituting the complex propagation constant $\tilde{\gamma} = \beta - j\alpha$ into Eq. (23) and conducting the singular value decomposition of the matrix $\mathbf{M}$, which is $\mathbf{M} = \mathbf{USV}^T$. The solution to the homogeneous system $\mathbf{Mx} = \mathbf{0}$ is the column vector of $\mathbf{V}$ corresponding to the smallest singular value. The values of R_i and T_i can be calculated correspondingly. The out-diffraction efficiency can be determined by first calculating the power flow in the z direction. The energy flux density is represented by the Poynting vector $\mathbf{S} = \frac{1}{2}\mathrm{Re}(\mathbf{E} \times \mathbf{H}^*)$, which can be reduced to $S_z = -\frac{1}{2}\mathrm{Re}(E_y H_x^*)$ for power flow in the z direction. The reflected power density and transmitted power density are calculated as

$$S_{z,i}^r = \frac{1}{2} R_i R_i^* \frac{\mathrm{Re}(k_{cz,i})}{\omega\mu_0}, \quad (34)$$

$$S_{z,i}^t = \frac{1}{2} T_i T_i^* \frac{\mathrm{Re}(k_{sz,i})}{\omega\mu_0}, \quad (35)$$

for $\mathrm{Re}(k_{cz,i}) < k_0 n_c$ and $\mathrm{Re}(k_{sz,i}) < k_0 n_s$, respectively. Otherwise, set $S_{z,i}^r$ and $S_{z,i}^t$ to zero. The preferential coupling ratios $PC_{c,i}$ and $PC_{s,i}$ of the ith order are defined as

$$PC_{c,i} = \frac{S_{z,i}^r}{\sum_i (S_{z,i}^r + S_{z,i}^t)}, \quad (36)$$

$$PC_{s,i} = \frac{S_{z,i}^t}{\sum_i (S_{z,i}^r + S_{z,i}^t)}. \quad (37)$$

Finally, the diffraction efficiencies $DE_{c,i}$ and $DE_{s,i}$ of the ith order at a given grating length ℓ are estimated by an exponential decaying distribution as

$$DE_{c,i} = PC_{c,i}[1 - \exp(-2\alpha\ell)], \quad (38)$$

$$DE_{s,i} = PC_{s,i}[1 - \exp(-2\alpha\ell)]. \quad (39)$$

C. Optimization and Validation

Given a set of parameters, such as the incident wavelength, waveguide thickness, grating height, grating period, and grating fill factor (grating profile), the above analysis directly gives the electric field distribution of the four-layer structure. Note that the fields calculated by RCWA are plane-wave fields. RCWA is not accurate for the situation in which the field is gradually building up or decaying away. But, using the radiation factor α, we can approximate decaying behavior of the field due to the existence of the grating. Since the grating is designed to couple the $i = +1$ order diffracted wave into the waveguide, $k_{x,+1}$ should be comparable to the fundamental propagation constant of the slab waveguide β_0. In this analysis, $k_{x,+1}$ is restricted to be in the range $|\beta_0 - k_{x,+1}| < k_0 n_w - \beta_0$. β_0 can be found using the method described in [34]. Briefly, the propagation constants of all possible propagating modes in the slab waveguide β_i are calculated by matching all tangential fields at the boundaries in a multilayer structure consisting of the cover, the waveguide, and the substrate. The propagation constant β_i is a function of the material refractive indices (n_c, n_w, n_s) and the waveguide thickness (t_w). If it exists, the fundamental mode β_0 is the one farthest from the cutoff, and thus will be considered in the analysis.

The present model is implemented in MATLAB and optimized using the function *fmincon*, available in the MATLAB optimization toolbox, which minimizes a function specified by a set of constraints. Specifically, inputs to the model are as follows: (1) the initial values of a set of undecided parameters [e.g., any combination of relative permittivity ϵ_r, incident wavelength λ, incident angle (or coupling angle) θ, grating profile (fill factor f or ridge location), grating period Λ, grating thickness t_g, and waveguide thickness t_w], (2) the lower and upper bounds of each parameter, (3) the function tolerance, and (4) the nonlinear constraint $|\beta_0 - k_{x,+1}| < k_0 n_w - \beta_0$. The model outputs the final values of those parameters that give the minimum value of $1 - DE_{c,+1}$, which corresponds to maximizing $DE_{c,+1}$.

In terms of validation, the optimized parameters can be first checked by the following criterion. For the $i = +1$ order to be coupled to the slab waveguide, $k_{x,+1}$ must be approximately equal to the fundamental mode propagation constant β_0 in the waveguide, as indicated in Fig. 3. Then, the optimized structure can be validated by 2D FDTD simulation. The FDTD simulation program used here is MEEP, a free software package developed at Massachusetts Institute of Technology (MIT).

3. RESULTS AND DISCUSSION

This model is capable of optimizing any parameters in a given configuration. In the analysis described here, a binary grating deposited on top of the waveguide is considered. For demonstration purposes, three parameters, namely grating period (Λ), grating height (t_g), and coupling angle (θ), are the variables to be optimized, and the other parameters are set as follows: free space wavelength $\lambda = 1.55$ μm, cover refractive index $n_c = 1$ (air), grating groove refractive index $n_{gr} = 1$ (air), grating ridge refractive index $n_{rd} = 2.46$ (Si_3N_4 [35]), waveguide refractive index $n_w = 3.45$ (Si [36,37]), substrate refractive index $n_s = 1.45$ (SiO_2 [35]), grating fill factor $f = 0.5$, waveguide thickness

Table 1. Optimized Parameters and Calculated Coupling Efficiency for Grating with Binary Rectangular Groove

Binary Case Number	Initial Guesses			Optimized Values						
	θ rad (deg)	Λ μm	t_g μm	θ rad (deg)	Λ μm	t_g μm	$PC_{c,+1}$	$DE_{c,+1}$ @$N = 50$	β μm^{-1}	α μm^{-1}
1	0.15 (8.59)	0.55	0.25	0.1761 (10.10)	0.5439	0.2337	0.5345	0.4417	10.8416	0.0322
2	0.20 (11.46)	0.55	0.25	0.2245 (12.86)	0.5462	0.2419	0.5474	0.5117	10.6020	0.0500
3	0.25 (14.32)	0.50	0.15	0.2499 (14.32)	0.5371	0.2071	0.5028	0.4812	10.6963	0.0301
4	0.15 (8.59)	0.55	0.10	0.1584 (9.08)	0.5701	0.2299	0.5328	0.4314	10.3822	0.0291
5	0.30 (17.19)	0.50	0.25	0.1014 (5.81)	0.5951	0.3555	0.8935	0.5142	10.1478	0.0144
6	0.25 (14.32)	0.50	0.30	0.2356 (13.50)	0.4845	0.3619	0.8295	0.5296	12.0212	0.0210
7	0.23 (13.18)	0.67	0.29	0.3137 (17.97)	0.5734	0.2836	0.6004	0.5718	9.7076	0.0531
8	0.20 (11.46)	0.80	0.25	0.2741 (15.70)	0.4968	0.2013	0.4690	0.3401	11.5492	0.0260
9	0.15 (8.59)	1.00	0.30	0.1479 (8.47)	0.6691	0.2629	0.4011	0.3115	8.7933	0.0224
10	0.10 (5.73)	0.70	0.25	0.3029 (17.35)	0.5919	0.2393	0.5000	0.2905	9.4064	0.0147

$t_w = 0.22$ μm. The fundamental mode propagation constant of the 0.22 μm thick waveguide is calculated to be $\beta_0 = 11.3710$ μm^{-1}. The total number of space harmonics is set to be $n = 7$. To ensure maximum coupling efficiencies, the +1 diffracted order is considered. The number of periods is set to $N = 50$. The optimization is carried out using the MATLAB function fmincon with the following constraints: (1) β_0 and $k_{x,+1}$ (propagation number of the +1 order in the x direction) should be numerically comparable, and thus we set the difference to be in the range $|\beta_0 - k_{x,+1}| < k_0 n_w - \beta_0$; (2) the value of α should be restricted so it is positive; and (3) the upper bounds and lower bounds of the three variables [Λ, t_g, θ] are set to be [1.55 μm, 0.4 μm, $\pi/4$ rad(45°)] and [0.3 μm, 0.05 μm, 0.1 rad (5.73°)], respectively. Taking into account fabrication limits, the thickness of the Si_3N_4 layer should be less than 0.4 μm [28], and the minimum coupling angle should be set to 0.1 rad (5.73°) to reduce the possibility of coupling into the −1 diffraction order. Due to the existence of local minima, the optimization may converge to different final values based on the choice of initial values (Λ, t_g, θ). It is recommended that several optimizations with different initial values should be chosen to ensure finding a global minimum. Please note the global minimum may vary depending on the constraints, which should be carefully evaluated according to specific needs. The optimization time depends on the choice of initial values as well as computer processor and memory. The computer used in this analysis has an Intel i5 CPU and 3.8 GB memory. All optimizations finished within 3 min.

Ten example optimized structures are summarized in Table 1. Each optimization starts with a set of initial values. If the initial values are far from the ideal values corresponding to the optimized structure (relatively large diffraction efficiencies), e.g., Cases 7–10, the RCWA-EIS method will still find the final values that are close to the ideal values, even though the diffraction efficiencies may not be maximized or accurate. Those final values can serve as rough estimates of the ideal values. If the initial values are in the vicinity of the ideal values, e.g., Case 1–5, the diffraction efficiencies found by the RCWA-EIS method are maximized and relatively accurate. Multiple optimizations should be carried out to ensure finding the global maximum diffraction efficiency, which is still computationally efficient due to the fast calculation of each optimization.

To give a better understanding of how the RCWA-EIS method works, the equivalent indices of Case 4 and Case 7 are summarized in Table 2. Case 4 illustrates an example that only requires four layers ($L = 4$) to achieve the function tolerance (<0.01). Case 7 is an example that requires five layers ($L = 5$). The equivalent indices of each layer may be any complex numbers without any physical meaning.

Generated by FDTD, Fig. 5 shows the grating-to-grating configuration using optimized designs. The distance between the gratings d is fixed at 1 μm. A waveguide mode at the frequency $c/\lambda_0 = 1.9355 \times 10^8$ Hz is launched from the left in the bottom waveguide. In order to calculate the interlayer grating coupling efficiency η, the input flux at the bottom waveguide and the output flux at the top waveguide need to be calculated. The single-grating diffraction efficiency ($DE_{c,+1}$)

Table 2. Equivalent Indices of Case 4 and Case 7 Calculated by the RCWA-EIS Method

Case 4 Equivalent Indices						
Iteration No.	**1st Layer**	**2nd Layer**	**3rd Layer**	**4th Layer**	**5th Layer**	**Func. Value**
1	1.1467–5.2892j	6.8679 + 1.5320j	5.9505–4.2526j	−3.0528–1.7341j	–	0.0002 < 0.01
Case 7 Equivalent Indices						
Iteration No.	**1st Layer**	**2nd Layer**	**3rd Layer**	**4th Layer**	**5th Layer**	**Func. Value**
1	0.7738–2.1118j	5.0964 + 1.1922j	4.3978–3.0027j	2.7236 + 1.8936j	–	0.0264 > 0.01
2	−0.9871 + 4.2330j	5.4118 + 1.3204j	3.6796–0.8072j	4.5069–2.4320j	2.5383 + 2.4434j	0.0020 < 0.01

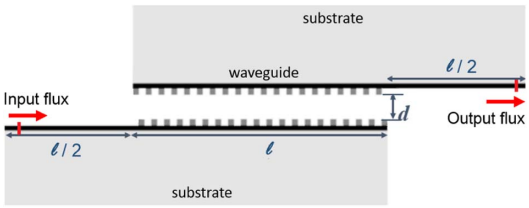

Fig. 5. Grating-to-grating structure generated by FDTD.

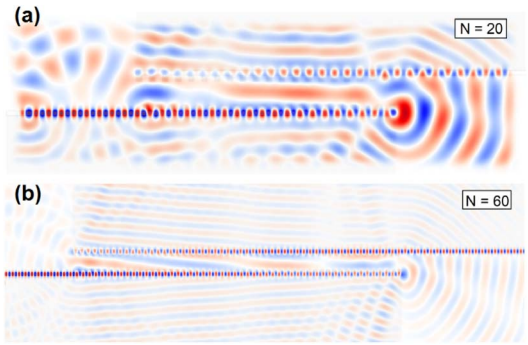

Fig. 6. FDTD simulations of an optimized binary grating with different numbers of periods: (a) $N = 20$ and (b) $N = 60$.

can be estimated by $\sqrt{\eta}$. The FDTD simulation results for Case 7 at grating lengths of 20 and 60 grating periods ($\ell = N \times \Lambda$, where $N = 20$ and 60) are shown in Figs. 6(a) and 6(b), respectively. The single-grating diffraction efficiencies as a function of grating length (or equivalently, number of grating periods N) calculated by the RCWA-EIS method and FDTD for Cases 2, 4, 6, and 7 are shown in Figs. 7(a)–7(d). To gain some insight into the effect of misalignment on interlayer grating coupling efficiencies, the top grating is shifted to the left with respect to the bottom grating by a distance corresponding to the coupling angle θ, and the FDTD simulation results of this shifted configuration are also shown in Figs. 7(a)–7(d).

From Fig. 6(a), it is observed that much of the power is lost at the end of the waveguide. This is due to the limited radiation associated with the short grating length. By increasing the grating length, most of the guided power is diffracted and coupled to the top waveguide, as indicated in Fig. 6(b). From the FDTD results, it is observed that the optimized structures, e.g., Cases 6 and 7, have diffraction efficiencies at about 55% at $N = 50$ or $\ell \approx 25$ μm. As grating length increases, the diffraction efficiencies approach 60%, which is limited by the preferential coupling ratio PC_c. The RCWA-EIS results demonstrate good agreement with FDTD results at large N, especially for Case 7, whose PC_c is about 0.6. The curves corresponding to the FDTD results oscillate at small N. This may due to two reasons: (1) at small grating lengths, the fields in the structures have not yet reached steady state, and thus the contribution of scattering at the waveguide ends becomes much more significant; (2) there is a stability issue in the FDTD calculation when a transient source, e.g., a Gaussian source (the input source in this work), is used, but as time increases, the nonphysical transients will decay. On the other hand, neither

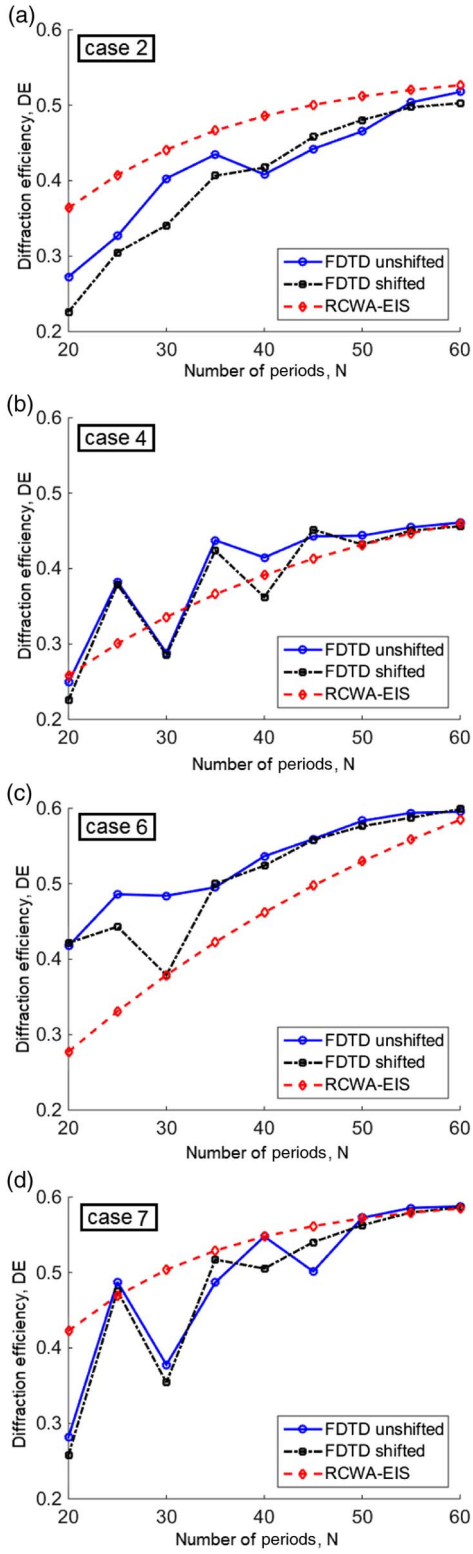

Fig. 7. Single-grating diffraction efficiency ($DE_{c,+1}$) as a function of the number of periods or the grating length ($\ell = N \times \Lambda$) for Cases 2, 4, 6, and 7.

the scattering effect nor the transient field is considered in the RCWA, and the RCWA-EIS method generates smooth curves as a result of the exponential mathematical model, Eq. (38).

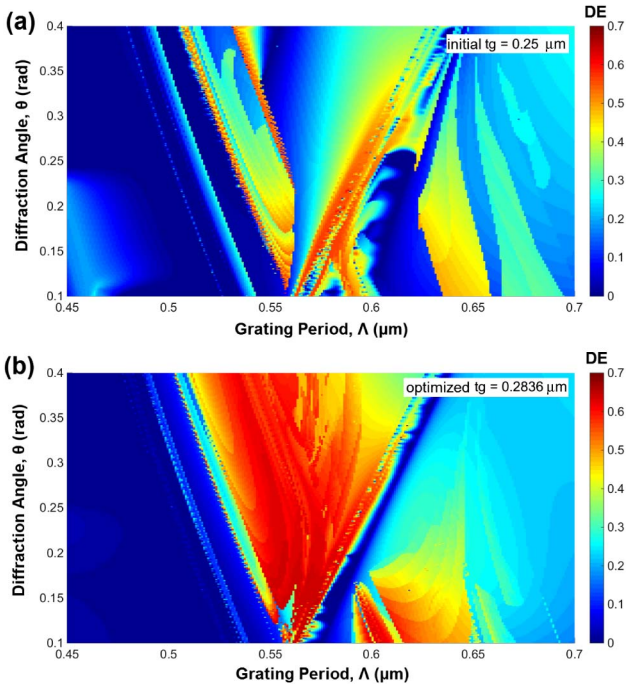

Fig. 8. Color map of the single-grating diffraction efficiency ($DE_{c,+1}$) with different grating thicknesses calculated at $N = 50$.

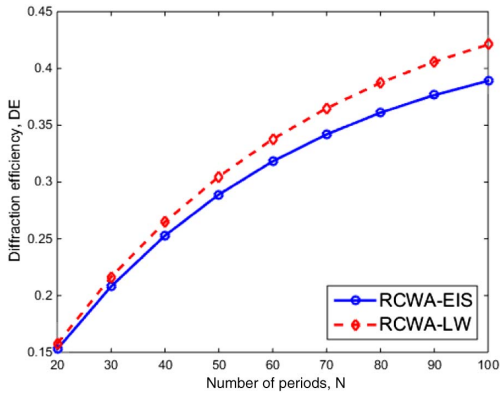

Fig. 9. Single-grating diffraction efficiency ($DE_{c,+1}$) as a function of the number of periods for a small-index-difference system. Both the RCWA-EIS and RCWA-LW approaches are effective in simulating systems with small-index differences.

Compared with the perfectly aligned configuration, the shifted configuration gives rise to similar FDTD results, offering the conclusion that a slight horizontal shift ($\approx d \tan\theta$) has little effect on the coupling efficiencies.

To better understand the effect of initial guesses on the final values, color maps of the single-grating diffraction efficiency are generated at fixed grating thicknesses $t_g = 0.25$ μm [a common initial guess, Fig. 8(a)] and $t_g = 0.2836$ μm [the optimized grating thickness in Case 7, Fig. 8(b)]. The diffraction efficiencies are calculated using the RCWA-EIS method at $N = 50$ grating periods. The mesh is set as follows: a grating period Λ from 0.45 μm to 0.7 μm with an increment of 0.001 μm, and a coupling angle θ from 0.1 rad (5.73°) to 0.4 rad (22.92°) with an increment of 0.001 rad (0.057°). In both color maps, only limited regions give rise to high diffraction efficiencies, and those efficiency "peaks" are distributed among efficiency "trenches." As a result, it is relatively difficult to find a global maximum because of this complicated "morphology." It is also observed that grating period and grating thickness are more influential on the efficiency than the coupling angle. Compared with Fig. 8(a), Fig. 8(b) shows a relatively larger high-efficiency area, which means the grating thickness $t_g = 0.2836$ μm is a better choice. Based on the RCWA-EIS calculation, the highest diffraction efficiency of the color map at $t_g = 0.2836$ μm is 0.6876, which is located at mesh point $\Lambda = 0.5650$ μm and $\theta = 0.1110$ rad(6.34°). According to the color map Fig. 8(b), this location is surrounded by many efficiency "trenches," making it difficult to reach.

Please note that the optimized structures are not restricted only to the cases demonstrated here. By varying initial guesses, multiple optimal parameter sets can be obtained. Due to the sensitive nature of the numerical problem, the RCWA-EIS method may obtain an extremely small or even negative α if the initial guesses are far from the ideal values. Even though those cases are avoided in the optimization process by setting constraints in the MATLAB *fmincon* function, the iteration may violate the constraints and gives erroneous results (extremely small or negative values). Again, this problem can be avoided by running multiple optimizations.

Finally, to further prove the validity of the RCWA-EIS method, its results for a small-index-difference system are compared with those generated by the RCWA-LW approach. The material system chosen is based on Papadopoulos and Glytsis [38]: $\lambda_0 = 1$ μm, $n_c = n_{gr} = 1$, $n_{rd} = n_w = 1.7321$, $n_s = 1.5166$, $f = 0.5$, $t_w = \lambda_0/\pi$, $t_g = 0.2\lambda_0$, $\Lambda = 0.5\lambda_0$, and $\theta = 0.4328$ rad(24.8°). The RCWA-EIS approach gives $\tilde{\gamma} = 9.9311 - 0.0212j$ μm^{-1} ($\alpha = 0.0212$ μm^{-1}) and $PC_{c,+1} = 0.4422$. As shown in Fig. 9, the diffraction efficiency $DE_{c,+1}$ calculated by the RCWA-EIS approach is plotted with respect to the number of periods N and compared with those calculated by the RCWA-LW approach. The plot corresponding to the RCWA-LW approach is generated by extracting data points from Fig. 9 of Papadopoulos and Glytsis [38]. Exponential curve fitting of the extracted data points gives $PC_{c,+1} = 0.4930$ and $\alpha = 0.0196$ μm^{-1}. The curves demonstrate good agreement at small N, while the relatively large offsets at larger N result from the difference in $PC_{c,+1}$ and α. Nevertheless, the offset is bounded by the difference in $PC_{c,+1}$, which is about 5%. It can be concluded that the RCWA-EIS approach is also effective in simulating systems with small-index differences.

4. CONCLUSIONS

In this work, optimization of interlayer grating coupling efficiency is achieved by the RCWA-EIS method introduced here. By assuming identical top and bottom gratings, the coupling efficiency is estimated by the single-grating diffraction efficiency based on the in-coupling process. The "equivalent index slab" method is proposed to solve the numerical instability in material systems with large-index differences. The advantages of this optimization method are: an arbitrary choice of grating

profile, fast calculation, wide parameter space search, easy implementation, and accurate results. The limitation of this method is that it can only optimize the +1 diffraction order due to the EIS approximation. The EIS method takes into account a limited number of the diffraction orders, whereas the RCWA-LW approach considers all of them. RCWA-EIS simplifies the evaluation of a large-dimension matrix in the RCWA-LW approach but reduces the capability to evaluate higher orders. Nevertheless, it is not necessary to optimize higher diffraction orders since the maximized diffraction efficiency is realized when the number diffracted orders is minimized. This method optimizes a given material system, but the coupling efficiency can be further improved by incorporating high-index coatings, reflective mirrors, overlays, etc., which are not considered here. In summary, the RCWA-EIS method is a useful tool for system designers to optimize the efficiency of interlayer grating structures.

REFERENCES

1. H. Kogelnik, "Coupled wave theory for thick hologram gratings," Bell Syst. Tech. J. **48**, 2909–2947 (1969).
2. A. Tishchenko, M. Hamdoun, and O. Parriaux, "Two-dimensional coupled mode equation for grating waveguide excitation by a focused beam," Opt. Quantum Electron. **35**, 475–491 (2003).
3. R. S. Chu and J. A. Kong, "Modal theory of spatially periodic media," IEEE Trans. Microwave Theory Tech. **25**, 18–24 (1977).
4. W. Streifer, D. R. Scifres, and R. D. Burnham, "Analysis of grating-coupled radiation in GaAs: GaAlAs lasers and waveguides-I," IEEE J. Quantum Electron. **12**, 422–428 (1976).
5. K. Ogawa, W. S. Chang, B. L. Sopori, and F. J. Rosenbaum, "A theoretical analysis of etched grating couplers for integrated optics," IEEE J. Quantum Electron. **9**, 29–42 (1973).
6. A. R. Neureuther and K. Zaki, "Numerical methods for the analysis of scattering from nonplanar periodic structures," Alta Freq. **38**, 282–285 (1969).
7. M. Nevière, R. Petit, and M. Cadilhac, "About the theory of optical grating coupler-waveguide systems," Opt. Commun. **8**, 113–117 (1973).
8. S. Peng, T. Tamir, and H. L. Bertoni, "Theory of periodic dielectric waveguides," IEEE Trans. Microwave Theory Tech. **23**, 123–133 (1975).
9. A. Zlenko, V. Kiselev, A. Prokhorov, A. Spikhal'skii, and V. Sychugov, "Emission of surface light waves from a corrugated part of a thin-film waveguide," Sov. J. Quantum Electron. **4**, 839–842 (1975).
10. V. Kiselev, "Diffraction coupling of radiation into a thin-film waveguide," Sov. J. Quantum Electron. **4**, 872–875 (1975).
11. V. A. Sychugov, A. V. Tishchenko, B. A. Usievich, and O. Parriaux, "Optimization and control of grating coupling to or from a silicon-based optical waveguide," Opt. Eng. **35**, 3092–3100 (1996).
12. A. Yariv, "Coupled-mode theory for guided-wave optics," IEEE J. Quantum Electron. **9**, 919–933 (1973).
13. A. Spikhal'skiĭ, V. A. Sychugov and A. V. Tishchenko, "Simple method for calculating the optical attenuation coefficient of a corrugated waveguide," Sov. J. Quantum Electron. **13**, 592–595 (1983).
14. M. G. Moharam, E. B. Grann, D. A. Pommet, and T. K. Gaylord, "Formulation for stable and efficient implementation of the rigorous coupled-wave analysis of binary gratings," J. Opt. Soc. Am. A **12**, 1068–1076 (1995).
15. T. K. Gaylord and M. Moharam, "Analysis and applications of optical diffraction by gratings," Proc. IEEE **73**, 894–937 (1985).
16. R. A. Villalaz, E. N. Glytsis, and T. K. Gaylord, "Volume grating couplers: polarization and loss effects," Appl. Opt. **41**, 5223–5229 (2002).
17. S. M. Schultz, E. N. Glytsis, and T. K. Gaylord, "Design of a high-efficiency volume grating coupler for line focusing," Appl. Opt. **37**, 2278–2287 (1998).
18. A. D. Papadopoulos and E. N. Glytsis, "Preferential-order waveguide grating couplers: a comparative rigorous analysis using the finite-difference time-domain method," Appl. Opt. **49**, 5787–5798 (2010).
19. R. Shi, H. Guan, A. Novack, M. Streshinsky, A. E.-J. Lim, G.-Q. Lo, T. Baehr-Jones, and M. Hochberg, "High-efficiency grating couplers near 1310 nm fabricated by 248-nm DUV lithography," IEEE Photon. Technol. Lett. **26**, 1569–1572 (2014).
20. B. Wohlfeil, L. Zimmermann, and K. Petermann, "Optimization of fiber grating couplers on SOI using advanced search algorithms," Opt. Lett. **39**, 3201–3203 (2014).
21. A. V. Mulé, R. Villalaz, T. K. Gaylord, and J. D. Meindl, "Quasi-free-space optical coupling between diffraction grating couplers fabricated on independent substrates," Appl. Opt. **43**, 5468–5475 (2004).
22. J. Kang, Y. Atsumi, Y. Hayashi, J. Suzuki, Y. Kuno, T. Amemiya, N. Nishiyama, and S. Arai, "Amorphous-silicon inter-layer grating couplers with metal mirrors toward 3-D interconnection," IEEE J. Sel. Top. Quantum Electron. **4**, 1–8 (2014).
23. M. Cabezón, I. Garcés, A. Villafranca, J. Pozo, P. Kumar, and A. Kaźmierczak, "Silicon-on-insulator chip-to-chip coupling via out-of-plane or vertical grating couplers," Appl. Opt. **51**, 8090–8094 (2012).
24. G. Li, Y. Hashimoto, T. Maruyama, and K. Iiyama, "High-efficiency optical coupling to planar photodiode using metal reflector loaded waveguide grating coupler," Opt. Quantum Electron. **45**, 657–663 (2013).
25. Y. Zhang, D. Kwong, X. Xu, A. Hosseini, S. Y. Yang, J. A. Rogers, and R. T. Chen, "On-chip intra-and inter-layer grating couplers for three-dimensional integration of silicon photonics," Appl. Phys. Lett. **102**, 211109 (2013).
26. S. Bernabé, C. Kopp, M. Volpert, J. Harduin, J.-M. Fédéli, and H. Ribot, "Chip-to-chip optical interconnections between stacked self-aligned SOI photonic chips," Opt. Express **20**, 7886–7894 (2012).
27. D. Vermeulen, S. Selvaraja, P. Verheyen, G. Lepage, W. Bogaerts, P. Absil, D. Van Thourhout, and G. Roelkens, "High-efficiency fiber-to-chip grating couplers realized using an advanced CMOS-compatible silicon-on-insulator platform," Opt. Express **18**, 18278–18283 (2010).
28. M. Sodagar, R. Pourabolghasem, A. A. Eftekhar, and A. Adibi, "High-efficiency and wideband interlayer grating couplers in multilayer Si/SiO_2/SiN platform for 3D integration of optical functionalities," Opt. Express **22**, 16767–16777 (2014).
29. R. Ulrich, "Efficiency of optical-grating couplers," J. Opt. Soc. Am. **63**, 1419–1431 (1973).
30. J. Harris, R. Winn, and D. Dalgoutte, "Theory and design of periodic couplers," Appl. Opt. **11**, 2234–2241 (1972).
31. M. G. Moharam, D. A. Pommet, E. B. Grann, and T. K. Gaylord, "Stable implementation of the rigorous coupled-wave analysis for surface-relief gratings: enhanced transmittance matrix approach," J. Opt. Soc. Am. A **12**, 1077–1086 (1995).
32. M. G. Moharam and T. K. Gaylord, "Diffraction analysis of dielectric surface-relief gratings," J. Opt. Soc. Am. **72**, 1385–1392 (1982).
33. S. Zhang and T. Tamir, "Analysis and design of broadband grating couplers," IEEE J. Quantum Electron. **29**, 2813–2824 (1993).
34. E. Anemogiannis and E. N. Glytsis, "Multilayer waveguides: efficient numerical analysis of general structures," J. Lightwave Technol. **10**, 1344–1351 (1992).
35. J. Kischkat, S. Peters, B. Gruska, M. Semtsiv, M. Chashnikova, M. Klinkmüller, O. Fedosenko, S. Machulik, A. Aleksandrova, G. Monastyrskyi, Y. Flores, and W. T. Masselink, "Mid-infrared optical properties of thin films of aluminum oxide, titanium dioxide, silicon dioxide, aluminum nitride, and silicon nitride," Appl. Opt. **51**, 6789–6798 (2012).
36. D. Pierce and W. Spicer, "Electronic structure of amorphous Si from photoemission and optical studies," Phys. Rev. B **5**, 3017–3029 (1972).
37. W. Primak, "Refractive index of silicon," Appl. Opt. **10**, 759–763 (1971).
38. A. D. Papadopoulos and E. N. Glytsis, "Optical waveguide grating couplers: 2nd-order and 4th-order finite-difference time-domain analysis," Appl. Opt. **48**, 5164–5175 (2009).